

## Correlation of Process Parameters and Layer Characteristics in High-Speed Directed Energy Deposition Using Optical Coherence Tomography

H. Wexel<sup>1</sup>, C. Krull<sup>2</sup>, P. Gajek<sup>1</sup>, S. Maffia<sup>3</sup>, T. Stittgen<sup>3</sup>, S. Koß<sup>2</sup>, J. Schleifenbaum<sup>2</sup> and F. Zanger<sup>1</sup>

<sup>1</sup>Karlsruhe Institute of Technology, wbk Institute of Production Science, Kaiserstr. 12, 76131 Karlsruhe, Germany

<sup>2</sup>RWTH Aachen University, Digital Additive Production (DAP), Campus-Boulevard 73, 52074 Aachen, Germany

<sup>3</sup>Ponticon GmbH, Alte Schmelze 20, 65201 Wiesbaden, Germany

### **Abstract**

High-speed directed energy deposition with laser beam (HS DED-LB) represents a key enabler for circular and resource-efficient production due to deposition velocities up to 200 m/min and layer heights down to 50 µm. To ensure process stability and product quality, precise in-situ monitoring techniques are required. This study investigates the application of Optical Coherence Tomography (OCT) as a high-resolution, non-contact method for real-time layer height measurement in HS DED-LB. By employing a Design of Experiments (DoE) in combination with response surface methodology (RSM), correlation models are derived that link key process parameters - laser power, processing speed, and powder mass flow rate - to layer height and relative density. The findings highlight the potential of OCT-based monitoring for early deviation detection in high-speed additive processes and to support the development of model-driven control approaches. This demonstrates its relevance for the optimization of resource-efficient additive manufacturing systems in circular production environments.

*Keywords:* High-Speed Directed Energy Deposition, Additive Manufacturing, Process Monitoring, Optical Coherence Tomography, OCT

### **1. Introduction**

In the context of increasing demands for sustainable and circular production, the extension of component lifetimes through remanufacturing is gaining strategic importance. Remanufacturing is defined as a value-retaining standardized process in which a remanufacturing product with at least the functionality and performance of the original product is created from reprocessed components [1]. For manufacturing reprocessing steps, a combination of subtractive and additive processes ensures maximum value retention through adaptation or compensation mechanisms [2]. Reprocessing not only reduces costs and downtime across various industries but also contribute significantly to resource efficiency and the implementation of circular economy principles [3–5].

Additive manufacturing (AM) plays a central role in this transformation, particularly powder-based directed energy deposition using a laser beam (DED-LB). This process enables the production and reprocessing of near-net-shape components by successively adding material. DED-LB is recognized as one of the key AM technologies for processing metal powders, alongside powder bed fusion with laser beam (PBF-LB) [6]. An advantage of DED-LB lies in its ability to

integrate multiple materials within a single component and to produce multifunctional structures. Additionally, 5-axis system configurations allow material deposition on complex surfaces. A particularly notable variant of this process is High-Speed Directed Energy Deposition with Laser Beam (HS DED-LB), also known by its German acronym EHLA (Extremes Hochgeschwindigkeits-Laserauftragsschweißen). In HS DED-LB, the powder stream is focused above the substrate, such that the powder particles are preheated and partially or fully melted before reaching the melt pool. This enables significantly higher processing speeds up to 200 m/min and reduced heat input compared to conventional DED-LB, which in turn leads to smaller melt pools and narrower heat-affected zones [7,8]. These characteristics not only shorten processing times but are also expected to enable the targeted adjustment of mechanical properties through precise control of powder–laser and powder–laser–substrate interaction times, potentially allowing for the fabrication of components with high hardness and strength. This makes HS DED-LB particularly suitable for applications in reprocessing and surface functionalization, meaning the modification, where the outer layer of a component is modified to improve properties such as wear resistance, corrosion resistance, or adhesion.

To fully leverage the potential of HS DED-LB in circular production environments, however, robust and precise process monitoring solutions are required. One of the key challenges in HS DED-LB is the precise control of the working distance, i.e., the gap between the nozzle outlet and the workpiece surface. Among the various approaches, Optical Coherence Tomography (OCT) has emerged as a promising solution. While OCT has been used in conventional DED processes for layer monitoring and even closed-loop control, its application in high-speed processes such as HS DED-LB remains largely unexplored.

## **2. State of the Art**

The outcome of the HS DED-LB process is significantly influenced by numerous parameters, including laser power, processing speed, and powder mass flow rate. Schaible et al. demonstrated that adjusting these parameters has a substantial effect on the process outcome [9], while different deposition strategies can further optimize the results [10]. In order to generate an understanding of the complex interactions in the HS DED-LB process, a sensory analysis of the process is beneficial. In their study, Wu et al. employed a welding camera equipped with a narrow bandpass filter to observe the melt pool dynamics on different substrates, demonstrating the dependence on process parameters and the effect of melt pool position on the outcome of the weld [11]. Schopphoven identified correlations between particle velocity and variables such as particle size, powder mass flow rate, and carrier gas flow rate, thereby highlighting the complexity of the process dynamics in the HS DED-LB process [5]. A study on thermal behavior of powder particles and melt pool as well as the resulting microstructure were conducted by Wang et al. Varying the laser focal plane and processing speed led to significant changes in the melt pool morphology [12].

In HS DED-LB multi-layer builds, cumulative thermal effects can induce progressive deviations in layer geometry, which, if not detected in time, may compromise part quality or lead to process failure [13]. Existing solutions for layer height control, such as layer-wise laser scanning or triangulation-based systems, often fail to meet the speed and robustness requirements of high-throughput processes like HS DED-LB [14,15]. In addition, the prediction of layer thickness using alternative monitoring variables, such as the size of the melt pool or temperature, poses significant challenges [15]. Optical Coherence Tomography offers a potential solution by enabling high-

resolution, non-contact and real-time measurement of the working distance. As demonstrated in [16,17], OCT has already shown its potential in conventional DED processes for process monitoring. Furthermore, OCT has also been successfully integrated into closed-loop control systems in DED [15]. However, its application in high-speed additive manufacturing environments remains largely unexplored. The present study addresses this gap by investigating the use of OCT for real-time layer height monitoring in HS DED-LB and evaluating its capability to support data-driven process control strategies. Although OCT enables precise measurement of the working distance, controlling this variable directly does not ensure consistent layer formation, which is required for consistent part quality. The objective of this study is to systematically investigate the influence of key process parameters - laser power, processing speed, and powder mass flow rate - on layer height and relative density in HS DED-LB using OCT-based in-situ measurements. A further aim is to derive correlation models that may serve as a basis for future model-driven process control.

### **3. Materials and Methods**

In this study, 1.4404 (316L) powder from m4p material solutions GmbH with a particle size ranging from 20  $\mu\text{m}$  – 63  $\mu\text{m}$  according to the manufacturer was deposited on a cold-rolled 1.0038 steel substrate. The powder was additionally analyzed by dynamic image analysis using a Camsizer X2 from Microtrac Retsch GmbH with regard to particle size distribution (PSD) and shape parameters.  $D_{10} = 21.1 \mu\text{m}$ ,  $D_{50} = 28.2 \mu\text{m}$ ,  $D_{90} = 35.9 \mu\text{m}$  and the SPAN value with  $\text{SPAN} = 0.523 \mu\text{m}$  were determined. Based on the sphericity of a particle, an equivalent diameter  $x_{c\_min}$  is calculated and the resulting count (index 0) or mass (index 3) is reported in a discrete (p) or cumulative (Q) manner. Figure 1 shows the PSD of the 1.4404 powder by particle mass.

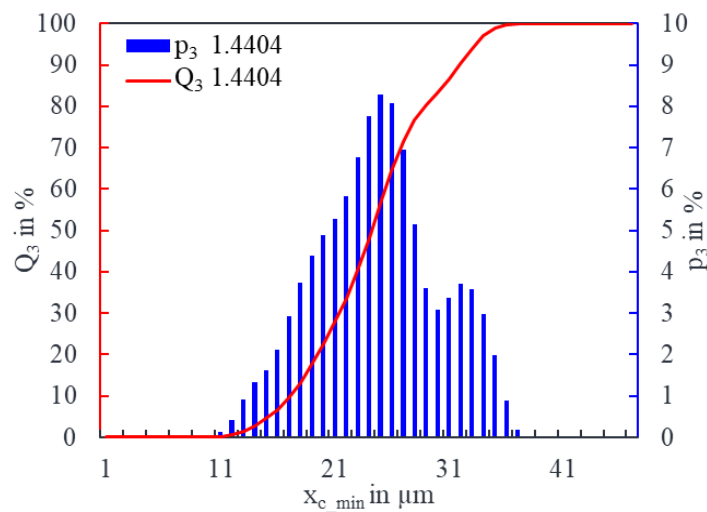


**Fig. 1.** Discrete and cumulative PSD by particle mass.

All experiments were conducted on a pE3D HS DED-LB system from Ponticon GmbH. The powder feeder used was a PF2-2 MFR model from BLC Lasercladding GmbH. A Laserline GmbH LDF 6000-40 high-power diode laser in conjunction with a Laserline GmbH RP13 coaxial powder nozzle were utilized. The working distance was determined by a coaxially integrated IDM1550 OCT optical sensor from Precitec GmbH & Co. Kg with a maximum sampling frequency

of 70 kHz, a measuring range from 134-14400  $\mu\text{m}$ , a linearity factor of 4.8  $\mu\text{m}$  and an operating wavelength of 1550 nm. In accordance with [14], the 20% percentile of the OCT readings is used to evaluate the layer height. The working principle and integration of the OCT in the HS DED-LB system can be derived from [14].

In this study, the process parameters laser power  $P_L$ , processing speed  $v$  and powder mass flow rate  $\dot{m}$ , were varied according to the Central Composite Design (CCD), based on a validated central point from a previous publication [18]. The levels -1 and 1 are set at approximately  $\pm 10\%$ . The resulting parameter combinations ( $\alpha = 1.7$ ) are presented in Table 1.

**Table 1.** Varied parameter combination according to the CCD.

Parameter combination n	$P_L$ in W	$v$ in m/min	$\dot{m}$ in g/min
1	2300	45	31.2
2	2100	50	28.18
3	1900	55	26.16
4	2300	55	26.16
5	1900	55	31.2
6	2300	55	31.2
7	1760	50	28.18
8	2430	50	28.18
9	2100	50	28.18
10	2100	41.5	28.18
11	2100	58.4	28.18
12	2100	50	28.18
13	1900	45	26.16
14	2300	45	26.16
15	1900	45	31.2
16	2100	50	23.1
17	2100	50	33.26

All samples were produced with an argon shielding gas flow rate  $\dot{V}_{sg} = 14$  l/min and an argon carrier gas flow rate  $\dot{V}_{cg} = 8$  l/min. The laser spot diameter was set to  $d_L = 1$  mm and the working distance from nozzle to substrate was  $WD = 14$  mm. For this parameter set, an optical examination of the powder-gas stream and evaluation of the 86% powder focus diameter  $d_{PF,86}$  according to [19] and the powder focus distance to the nozzle were performed using the PowderSpy from Ponticon GmbH. As can be seen from Fig. 2, the selected process parameters result in the formation of a uniform powder-gas cone and powder focus. The yellow dashed line shows the position of the substrate as well as the position of the powder focus (red dashed line).

Cuboid samples with a base area of 8 mm  $\times$  30 mm were produced, with a track spacing of  $s = 0.4$  mm and  $n = 25$  layers. The relative density was determined for each parameter combination. In order to ensure that all samples for this study were produced at a constant working distance, the layer height was identified in advance using OCT monitoring. Therefore, a tolerance band of  $\pm 0.25$  mm around the nominal working distance of 14 mm was defined, allowing a maximum of 4 out of 25 layers per sample to deviate beyond this range. Thus, each parameter set is assigned a layer height and density value, which serve as input for the subsequent modelling.

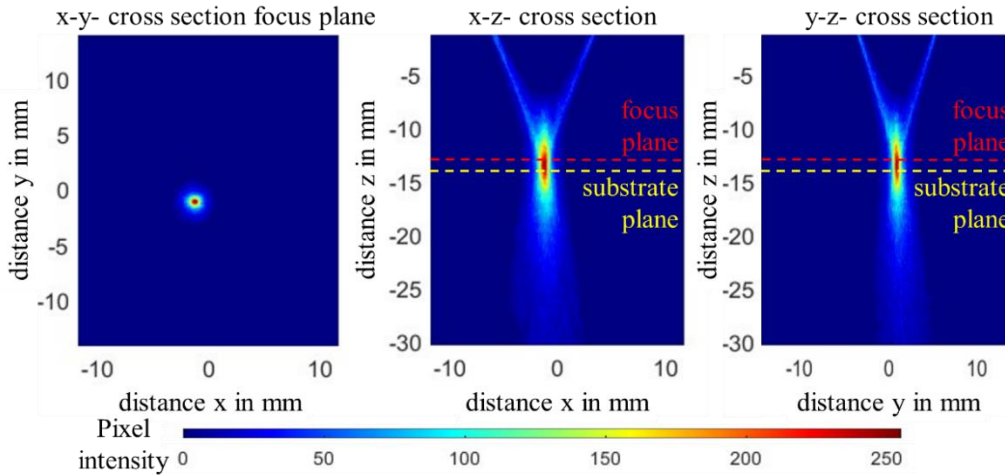


**Fig. 2.** Optical examination of the powder-gas stream with the PowderSpy.

In the framework of response surface methodology (RSM), a second-order polynomial is used to capture potential nonlinear relationships (Equation 1). The model includes linear, quadratic, and interaction terms for the three input variables laser power ( $x_1$ ), process speed ( $x_2$ ), and powder mass flow rate ( $x_3$ ), while the output responses  $S$  are defined as relative density and layer height. The resulting regression equation is expressed as:

$$S = a_0 + a_1 * x_1 + a_2 * x_2 + a_3 * x_3 + a_{11} * x_1^2 + a_{22} * x_2^2 + a_{33} * x_3^2 + a_{12} * x_1 * x_2 + a_{13} * x_1 * x_3 + a_{23} * x_2 * x_3 \quad \text{Eq. 1}$$

Model coefficients are determined using the partial least squares (PLS) regression method. The resulting regression models are evaluated and refined using analysis of variance (ANOVA) to assess the statistical significance of individual model terms. Through backward elimination, non-significant terms are systematically removed to obtain a reduced model containing only statistically relevant predictors. The quality of the resulting model is subsequently assessed using standard statistical metrics that evaluate its goodness of fit. The model's generalizability is validated using support points from a full factorial design with  $\pm 5\%$  variation around central values. Residuals between predicted and measured working distances are analyzed to assess interpolation accuracy within the defined parameter space.

## **4. Results and Discussion**

### **Monitoring of the layer height**

The results of the OCT values from the center point tests (parameter combinations 2, 9 and 12) demonstrate that identical working distance curves are achieved across the number of layers (Figure 3), thereby demonstrating a high degree of repeatability was achieved across the test plan. It is notable that the shift in the values of  $n_2$  can be attributed to an initially deviating working distance setting. This enables modelling with correlation models within a limited parameter space, which is useful for improving process understanding and developing a basis for control.

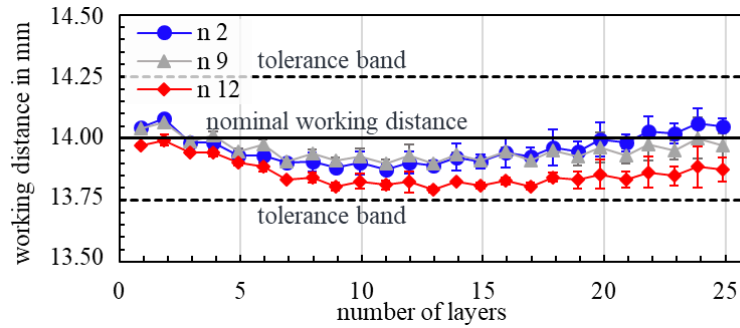


**Figure 3.** Results of in situ monitoring of the working distance of the center point tests.

The results of in situ monitoring of the working distance using OCT can be divided into four distinct cases, as illustrated in Figure 4. In order to circumvent the impact of the outer tracks on the mean layer height, the standard deviations presented are based on the mean of the values from tracks 5 to 15.

- The working distance of parameter combinations 1, 7 and 10 decreases until approximately the eighth layer, at which point it increases at different rates. Consequently, the working distance increases from layer eight onwards.
- The working distance demonstrates a comparable trend to the tests in a), with the exception that the working distance remains constant at the beginning for parameter combinations 4, 13 and 17. From layer 15 an increase in the working distance is observed. It is evident that the standard deviations are increased in subsequent layers in comparison to the initial layers. Similar results are obtained with parameter combinations 6, 8 and 15.
- For parameter combinations 3, 5 and 11, the values of the first layer are close to 14 mm. However, the working distance decreases to approximately the tenth layer and then remains almost constant between 13.8 mm and 13.9 mm.
- Parameter combinations 14 and 16 show only minor fluctuations in working distance, remaining within a 120  $\mu\text{m}$  range throughout the process.

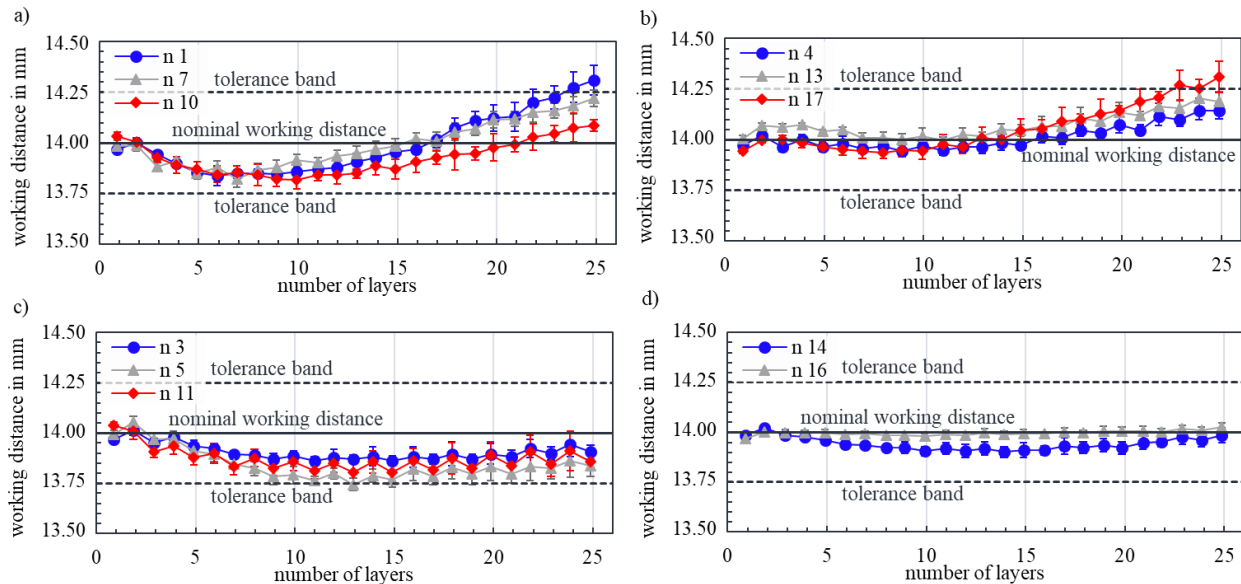


**Fig. 4.** Results of in situ monitoring of the working distance using OCT.

Based on a qualitative evaluation of the OCT data, no clear trend can be observed that links the variation in process parameters to the progression of the working distance over the number of layers. Nevertheless, it is noticeable that either the working distance remains almost constant with an increasing number of layers (Figure 4 c), d)), or it becomes larger (Figure 4 a), b)). Donadello et al. argue that the DED process may possess a self-stabilizing range, which is only achieved when the average layer height exceeds the selected Z increment. This assumption is based on the observation that the layer height decreases when the working distance is too low, resulting in self-regulation [20]. This assumption is particularly supported by Figure 4 c). In many of the experiments conducted, the increase in working distance with an increasing layer count is due to the change in shape of the manufactured component as its height increases. The rounded shape of the component reduces the layer height at the outer tracks, thereby reducing the average layer height. This is also evident from the larger standard deviations of the later layers (Figure 4 a), b)).

Figure 5 shows the layer heights evaluated using OCT and the aforementioned method for each parameter combination. The maximum layer height of  $h = 186 \mu\text{m}$  is achieved with parameter combination n 1 with the highest linear energy. The center point samples have a mean layer height of  $155 \mu\text{m}$ , with a standard deviation of  $2.9 \mu\text{m}$ . Subsequently, the mean value of the center points is utilized for the modelling.

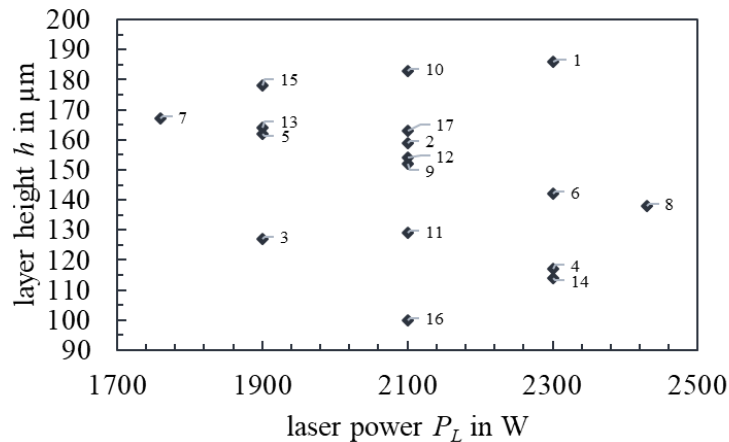


**Fig. 5.** Evaluated layer height per parameter combination based on OCT measurements.

### Density evaluation

Exemplary cross sections of the cuboid samples with the lowest and the highest linear energy density are depicted in Figure 6. The relative density results for all parameter combinations of the optical analysis for the cuboids are shown in Figure 7. The maximum relative density of 99.95% is achieved with n 1. Parameter combination 3 produces the lowest density of 99.29%. The center point samples have a mean relative density of 99.74%, with a standard deviation of 0.05%.

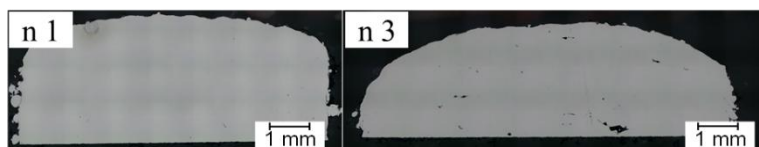


**Fig. 6.** Cross sections of samples a) n 1 with the highest linear energy (2100 W, 45 m/min) and b) n 3 with the lowest linear energy (1900 W, 55 m/min).

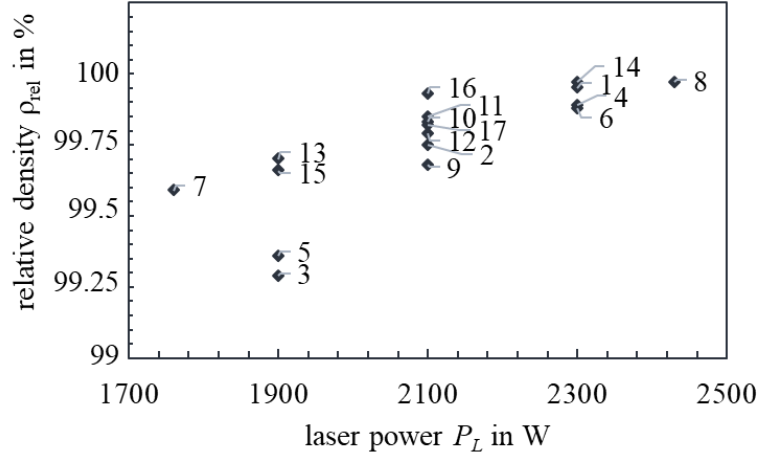


**Fig. 7.** Relative density of all cuboid samples obtained via optical analysis.

### Modelling based on layer height and density evaluation

Two mathematical equations were derived using regression analysis to describe the effect of varying process parameters on layer height in  $\mu\text{m}$  (Equation 2) and relative density in % (Equation 3), based on the obtained findings. The process parameters in the equations are scaled as follows: laser power  $P_L$  in watts (W), processing speed  $v$  in millimeters per second (mm/s), and mass flow rate  $\dot{m}$  grams per minute (g/min).

$$\begin{aligned}
 h = & 75 - 0.376 * P_L - 4.0 * v + 42.7 * \dot{m} \\
 & - 0.000004 * P_L^2 + 0.042 * v^2 - 0.829 * \dot{m}^2 \\
 & + 0.0015 * P_L * v + 0.00993 * P_L * \dot{m} - 0.215 * v * \dot{m}
 \end{aligned} \tag{Eq. 2}$$

$$\begin{aligned}
 \rho_{rel} = & 106.5 - 0.00061 * P_L - 0.197 * v + 0.123 * \dot{m} \\
 & + 0 * P_L^2 + 0.001 * v^2 - 0.00168 * \dot{m}^2 \\
 & + 0.00007 * P_L * v + 0.000012 * P_L * \dot{m} - 0.00099 * v * \dot{m}
 \end{aligned} \tag{Eq. 3}$$

The equations are analyzed and evaluated using key figures from a multivariate ANOVA. The two essential categories used for this evaluation are shown in Table 2. Corrected sum of squares  $Cor_{ss}$  refers to the sum of squared deviations between observed and predicted layer heights, accounting for the number of parameters in the model. The  $p$ -value is a statistical measure used to reject or accept the null hypothesis. Regarding the layer height model, the total value of the  $Cor_{ss\_h}$  data is 10013.3, of which the model describes 9351.7, resulting in a remaining error of 661.6. The largest proportion of the modelled  $Cor_{ss\_h}$  values can be attributed to the linear terms (8164.7), and in particular to the linear term of the powder mass flow rate (4583.5). The  $p$ -values $\_h$  of the individual terms adhere to this logic and describe all linear terms as significant for the model ( $p$ -value $\_h < 0.1$ ). The next smallest  $p$ -value $\_h = 0.167$ , is attributed to the quadratic mass flow. The overall model demonstrated a  $p$ -value $\_h$  of 0.018, indicating a statistically significant result. For the density model, the  $Cor_{ss\_rho_{rel}}$  is 0.62, of which the model describes 0.495. This results in an error of 0.129. The linear laser power term has the strongest influence on relative density ( $Cor_{ss\_rho_{rel}} = 0.39$ ) and is the only statistically significant factor at the  $p$ -values $\_rho_{rel} < 0.1$  level.

**Table 2.** ANOVA of the entire quadratic layer height and density model.

Source	<i>Cor<sub>ss</sub> h</i>	<i>p-value h</i>	<i>Cor<sub>ss</sub> ρ<sub>rel</sub></i>	<i>p-value ρ<sub>rel</sub></i>
model	9351.7	0.018	0.495751	0.209
<b>linear</b>	8164.7	0.003	0.446989	0.044
P <sub>L</sub>	1067.0	0.036	0.391353	0.011
v	2517.3	0.007	0.052971	0.212
$\dot{m}$	4583.5	0.002	0.002490	0.769
<b>quadratic</b>	734.2	0.256	0.007920	0.955
P <sub>L</sub> <sup>2</sup>	0.3	0.965	0.001551	0.816
v <sup>2</sup>	6.8	0.829	0.000037	0.971
$\dot{m}^2$	346.3	0.167	0.001417	0.842
<b>two-factor interaction</b>	390.5	0.471	0.041450	0.678
P <sub>L</sub> *v	18.0	0.727	0.039200	0.273
P <sub>L</sub> * $\dot{m}$	288.0	0.200	0.00450	0.900
v* $\dot{m}$	84.5	0.260	0.001800	0.802
<b>error</b>	661.6	-	0.129089	-
<b>total</b>	10013.3	-	0.624840	-

For the entire layer height model,  $R^2 = 93.39$  and  $R^2_{\text{prog}} = 18.16$ . For the entire density model,  $R^2 = 79.34$  and  $R^2_{\text{prog}} = 0.0$ . The significant difference between  $R^2$  and  $R^2_{\text{prog}}$  indicates that the models are overfitted. In order to reduce overfitting while achieving a low standard deviation and a high degree of goodness of fit, terms with a significance level of 0.1 were eliminated using backward elimination. Therefore, the coefficient of determination  $R^2$  for Equation 4 is 89.35%, while the  $R^2_{\text{prog}}$  is 78.6%. For Equation 5  $R^2 = 71.04$  and  $R^2_{\text{prog}} = 53.12$ . While the predictive quality of the density model remains limited, the following analysis provides initial insight into the parameter influence and identifies the need for an extended process window and refined modelling approaches.

$$h = -475 - 0.442 * P_L - 2.702 * v + 54.8 * \dot{m} - 0.865 * \dot{m}^2 \quad \text{Eq. 4}$$

$$\rho_{\text{rel}} = 98.58 - 0.000851 * P_L - 0.01207 * v \quad \text{Eq. 5}$$

**Table 3.** ANOVA of the layer height and density model after backward elimination.

Source	<i>Cor<sub>ss</sub> h</i>	<i>p-value h</i>	<i>Cor<sub>ss</sub> ρ<sub>rel</sub></i>	<i>p-value ρ<sub>rel</sub></i>
model	8946.8	0.000	0.44387	0.001
<b>linear</b>	8216.8	0.000	0.44387	0.001
P <sub>L</sub>	1065.4	0.010	0.39391	0.000
v	2503.2	0.001	0.04997	0.094
$\dot{m}$	4648.2	0.000	-	-
<b>quadratic</b>	719.8	0.027	-	-
$\dot{m}^2$	719.8	0.027	-	-
<b>error</b>	1066.5	-	0.18097	-
<b>total</b>	10013.3	-	0.62484	-

Table 3 presents the results of the ANOVA of the adjusted models. With regard to layer height, the error has increased by approximately 400 compared to the ANOVA of the initial model (see Table 2), which is due to the omitted terms. The error of the density model has increased by 0.05. The *p-values* of the remaining terms are all below the set significance level of 0.1, and thus are considered to be statistically significant.

Figure 8 shows the main effects of the varied parameters on the layer height derived from Equation 4. The decrease in layer height with increasing laser power may be attributable to the heating of particles above their vaporization temperature prior to contact with the substrate at higher laser powers. Schopphoven simulated the behavior of particles in an HS DED-LB process with a mass flow of 15 g/min and a processing speed of 100 m/min. At a laser power of 2 kW, 5% of the particles were found to be heated above their evaporation temperature [5]. Furthermore, Wu et al. also observed a decrease in layer height once a certain surface energy density was exceeded [21]. Yan et al. investigated the effect of increasing laser power on track width. If the track widens, the layer height must decrease at a constant melting output [22]. Schopphoven explains this observation in the HS-DED-LB process by the fact that, due to the high particle temperature, a proportion of particles form a metallurgical bond despite not ending up in the comparatively small melt pool. These particles attach to the side of the layer, thereby increasing the track width [5]. The correlation between layer height and processing speed, as illustrated in Figure 8 b), is consistent with the findings reported in the existing literature [21,23]. As the processing speed increases, the interaction time between the laser and the powder with the substrate is reduced. The resulting reduction in the amount of powder and energy introduced results in a reduced layer height. The most significant variations in layer height is caused by variations in the powder mass flow rate. This influence has been confirmed many times in scientific studies [5,24]. The quadratic term in Equation 4 (shown in Figure 8 c)) arises because, above a certain mass flow rate, there is insufficient laser radiation to melt the substrate adequately. Additionally, the proportion of powder particles that are completely melted decreases [5].

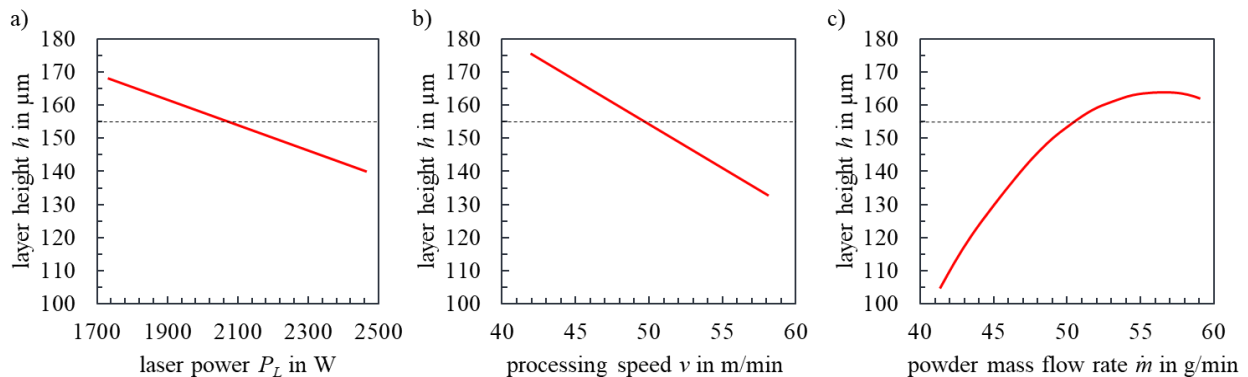


**Fig. 8.** Main effects of the a) laser power, b) processing speed and c) powder mass flow rate on the layer height. The dashed line indicates the mean layer height at center point conditions.

In order to enable OCT-based control, the parameters must be examined as control variables. While mass flow would be the logical choice based on the above relationships, additional considerations regarding the responsiveness, meaning the speed at which the parameter can be adapted in situ and the resulting complexity must be considered.

The responsiveness of the powder mass flow rate varies greatly depending on the HS DED-LB system and cannot be quantified in general terms. However, it should be noted that changes in mass flow have dead times of several seconds. Conversely, the low response time of the laser ( $\ll 1$  s) results in a short control time, but its influence on the layer height is relatively minor. The processing speed cannot be controlled as quickly as the laser power and is also more complex, as acceleration and deceleration processes must be considered, particularly with more complex geometries. Nevertheless, the impact on the layer height is greater in comparison to that of the laser power. Due to the high dynamics of the HS DED-LB process, a high rate of change of the control variable is essential. This means that the powder mass flow rate is currently unsuitable as a key control variable. However, the findings thus far indicate that the laser power and processing speed are suitable for integration into a future process control system. While the effects on layer height are less pronounced than those achieved by adjusting the powder mass flow rate, they are considered sufficient for the HS DED-LB process.

To control the HS DED-LB process, not only is a defined layer height required, but also a layer with the highest possible density, as density has a major influence on the mechanical properties of the component. Figure 9 shows the main effects of the varied parameters on the density derived from Equation 5.

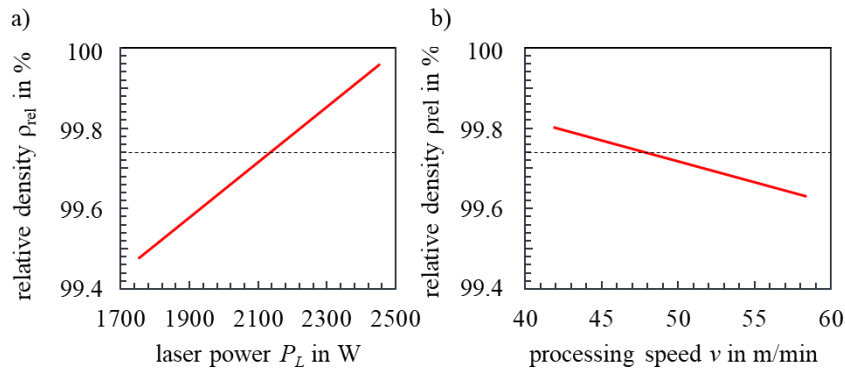


**Fig. 9.** Main effects of the parameters a) laser power and b) processing speed on the relative density. The dashed line indicates the mean relative density at center point conditions.

The density model should be viewed critically, given that it produces unphysical densities of over 100%, as well as having low coefficients of determination and comparatively high standard deviations. Nevertheless, the coefficient of determination ( $R^2 = 71.04\%$ ) indicates that the model captures the main trends within the investigated parameter space. The approximately linear response behavior supports its use for interpolation within this range. However, extrapolation beyond the tested process window is not recommended. Depending on the energy input, different defects can occur in the HS DED-LB process. Insufficient energy input results in lack of fusion pores, whereas excessive energy input leads to keyhole pores [18,25]. Lack of fusion defects can be seen in the cross-section of sample n 3 (low line energy density). Sample n 1, which has the highest linear energy density, has almost no pores. Therefore, it can be assumed that the energy inputs of the selected parameter combinations are just below the transition to the lack of fusion range. Further work is therefore required to extend the parameter window to higher linear energy densities to improve the density model.

### Validation of the layer height model

The layer height model is validated using a full-factorial test plan, with modelled ( $h_{mod}$ ) and measured ( $h_{meas}$ ) values shown in Table 4.

**Table 4.** Test plan for model validation with modelled and measured layer height.

Parameter combination n	$P_L$ in W	$v$ in m/min	$\dot{m}$ in g/min	$h_{mod}$ in $\mu\text{m}$	$h_{meas}$ in $\mu\text{m}$	absolute difference in $\mu\text{m}$	relative difference in %
18	2200	47.5	26.65	144	144	0	0
19	2000	52.5	29.88	159	151	-8	5.3
20	2200	52.5	26.65	131	124	-7	5.6
21	2000	52.5	26.65	140	132	-8	6.1
22	2000	47.5	26.65	153	147	-6	4.1
23	2200	52.5	29.88	150	145	-5	3.4
24	2200	47.5	29.88	164	158	-6	3.8
25	2000	47.5	29.88	172	170	-2	1.2
26	2100	50	28.18	153	152	-1	0.7

The difference between the modelled and measured layer heights is a maximum of 8  $\mu\text{m}$ . With the exception of n 18, all differences are negative, meaning that the modelled layer height is higher than the actual layer height. The relative error refers to the measured layer height and takes values in the range 0% - 6.1%. The results confirm the hypothesis that the layer height model describes the correlation between the input variables and the layer height within the parameter space. The fact that the absolute difference is always  $\leq 0$  can be explained by the service life of the nozzle. The validation experiments were conducted at a later stage (approximately two months) than the model development, which may introduce effects such as nozzle wear or system drift. While redeveloping the model and validating it within a closer time window could improve alignment, this was beyond the scope of the present study. Nevertheless, the observed prediction accuracy confirms the robustness of the approach.

## **6. Conclusion and Outlook**

This study has demonstrated the feasibility and potential of using Optical Coherence Tomography (OCT) for high-resolution, real-time monitoring of the layer height in High-Speed Directed Energy Deposition with Laser Beam (HS DED-LB). By linking OCT-based measurements with varied process parameters, correlation models were derived that enable a quantitative understanding of their influence on both layer height and relative density. The regression model for layer height showed a high degree of accuracy and generalizability within the defined parameter space, as confirmed by validation experiments. These results highlight the capability of OCT not only as a monitoring tool, but also as a valuable sensor input for model-driven process control strategies. However, the results also reveal limitations in predicting relative density, indicating the need for further refinement of the modelling approach and an expansion of the parameter space, particularly towards higher energy densities. Moreover, while powder mass flow rate emerged as the dominant factor affecting layer height, its dynamic controllability in real-world systems remains restricted. In contrast, laser power and process speed, although less influential, offer practical advantages in terms of responsiveness for in-situ control.

Building on these findings, future work should focus on the integration of OCT-based measurements into a closed-loop control framework for HS DED-LB, allowing real-time adjustment of laser power or process speed to maintain stable build conditions. Moreover, future work should explore ways to increase the powder mass flow response time, as it was the most influential factor for layer height. In addition, an extended study of defect formation mechanisms and their relation to process signatures will support the development of more robust density models. Ultimately, these advances will contribute to the realization of intelligent, resource-efficient additive manufacturing systems suitable for circular production environments.

**Acknowledgment** Funded by the German Research Foundation (DFG, German Research Foundation) - SFB-1574 – 471687386.

## References

- [1] DIN SPEC 91472:2023-06, Remanufacturing (Reman)\_ - Qualitätsklassifizierung für zirkuläre Prozesse, (n.d.). <https://doi.org/10.31030/3434252>.
- [2] G. Lanza, B. Deml, S. Matthiesen, M. Martin, O. Brützel, R. Hörsting, The vision of the circular factory for the perpetual innovative product, *At - Automatisierungstechnik* 72 (2024) 774–788. <https://doi.org/10.1515/auto-2024-0012>.
- [3] Z. Tang, W. Liu, Y. Wang, K.M. Saleheen, Z. Liu, S. Peng, Z. Zhang, H. Zhang, A review on in situ monitoring technology for directed energy deposition of metals, *Int J Adv Manuf Technol* 108 (2020) 3437–3463. <https://doi.org/10.1007/s00170-020-05569-3>.
- [4] J. Bennett, D. Garcia, M. Kendrick, T. Hartman, G. Hyatt, K. Ehmann, F. You, J. Cao, Repairing Automotive Dies With Directed Energy Deposition: Industrial Application and Life Cycle Analysis, *Journal of Manufacturing Science and Engineering* 141 (2019) 021019. <https://doi.org/10.1115/1.4042078>.
- [5] T. Schopphoven, Experimentelle und modelltheoretische Untersuchungen zum Extremen Hochgeschwindigkeits-Laserauftragschweißen, 2019.
- [6] A. Bagherzadeh, E. Budak, E. Ozlu, B. Koc, Machining behavior of Inconel 718 in hybrid additive and subtractive manufacturing, *CIRP Journal of Manufacturing Science and Technology* 46 (2023) 178–190. <https://doi.org/10.1016/j.cirpj.2023.08.004>.
- [7] A. Singh, S. Kapil, M. Das, A comprehensive review of the methods and mechanisms for powder feedstock handling in directed energy deposition, *Additive Manufacturing* 35 (2020) 101388. <https://doi.org/10.1016/j.addma.2020.101388>.
- [8] S. Greco, M. Schmidt, K. Klauer, B. Kirsch, J.C. Aurich, Hybrid manufacturing: influence of material properties during micro milling of different additively manufactured AISI 316L, *Prod. Eng. Res. Devel.* 16 (2022) 797–809. <https://doi.org/10.1007/s11740-022-01139-6>.
- [9] J. Schaible, L. Sayk, T. Schopphoven, J.H. Schleifenbaum, C. Häfner, Development of a high-speed laser material deposition process for additive manufacturing, *Journal of Laser Applications* 33 (2021) 1–9. <https://doi.org/10.2351/7.0000320>.
- [10] J. Schaible, D. Hausch, T. Schopphoven, C. Häfner, Deposition strategies for generating cuboid volumes using extreme high-speed directed energy deposition, *Journal of Laser Applications* (2022) 1–9. <https://doi.org/10.2351/7.0000770>.
- [11] Z. Wu, P. O’Toole, C. Hagenlocher, M. Qian, M. Brandt, J. Watts, Melt pool dynamics on different substrate materials in high-speed laser directed energy deposition process, *Journal of Laser Applications* 35 (2023). <https://doi.org/10.2351/7.0001145>.
- [12] K. Wang, X. Yin, C. Li, K. Du, M. Halifu, Study on the thermal behavior and microstructure of Fe-based deposited layers prepared by laser cladding on Al substrate,

- Optics & Laser Technology 179 (2024) 111365.  
<https://doi.org/10.1016/j.optlastec.2024.111365>.
- [13] S. Donadello, M. Motta, A.G. Demir, B. Previtali, Monitoring of laser metal deposition height by means of coaxial laser triangulation, *Optics and Lasers in Engineering* 112 (2019) 136–144. <https://doi.org/10.1016/j.optlaseng.2018.09.012>.
- [14] S. Maffia, C. Krull, T. Stittgen, H. Wexel, F. Zanger, S. Koß, J.H. Schleifenbaum, Optical Coherence Tomography (OCT) for Real-time Layer Thickness Monitoring in High-speed Laser Metal Deposition Process, *Berg Huettenmaenn Monatsh* 170 (2025) 179–187. <https://doi.org/10.1007/s00501-025-01564-x>.
- [15] S. Maffia, V. Furlan, B. Previtali, Coaxial and synchronous monitoring of molten pool height, area, and temperature in laser metal deposition, *Optics & Laser Technology* 163 (2023) 109395. <https://doi.org/10.1016/j.optlastec.2023.109395>.
- [16] J. Kittel, F. Wendt, S. Hoelters, A. Gasser, M. Hackel, Approach for advanced working distance monitoring and control capability in laser metal deposition processing for additive manufacturing, *Journal of Laser Applications* 35 (2023) 022032. <https://doi.org/10.2351/7.0000886>.
- [17] C. Stehmar, M. Gipperich, M. Kogel-Hollacher, A. Velazquez Iturbide, R.H. Schmitt, Inline Optical Coherence Tomography for Multidirectional Process Monitoring in a Coaxial LMD-w Process, *Applied Sciences* 12 (2022) 2701. <https://doi.org/10.3390/app12052701>.
- [18] H. Wexel, P. Fischmann, J. Schubert, F. Zanger, High-Speed DED-LB: Analysis of Process Control Variables as Enabler for Remanufacturing of Unique Products, *Procedia CIRP* 127 (2024) 230–235. <https://doi.org/10.1016/j.procir.2024.07.040>.
- [19] Z. Jardon, P. Guillaume, J. Ertveldt, M. Hinderdael, G. Arroud, Offline powder-gas nozzle jet characterization for coaxial laser-based Directed Energy Deposition, *Procedia CIRP* 94 (2020) 281–287. <https://doi.org/10.1016/j.procir.2020.09.053>.
- [20] S. Donadello, V. Furlan, A.G. Demir, B. Previtali, Interplay between powder catchment efficiency and layer height in self-stabilized laser metal deposition, *Optics and Lasers in Engineering* 149 (2022) 106817. <https://doi.org/10.1016/j.optlaseng.2021.106817>.
- [21] Z. Wu, M. Qian, M. Brandt, N. Matthews, Ultra-High-Speed Laser Cladding of Stellite® 6 Alloy on Mild Steel, *JOM* 72 (2020) 4632–4638. <https://doi.org/10.1007/s11837-020-04410-2>.
- [22] Q. Yan, K. Yang, Z. Wang, M. Chen, G. Sun, Z. Ni, Surface roughness optimization and high-temperature wear performance of H13 coating fabricated by extreme high-speed laser cladding, *Optics & Laser Technology* 149 (2022) 107823. <https://doi.org/10.1016/j.optlastec.2021.107823>.
- [23] Z. Yong, L. Chang, S. Jiang, D. Xie, F. Xing, H. Shen, L. Shen, Z. Tian, Parameter optimization of T800 coating fabricated by EHLA based on response surface methodology, *Optics & Laser Technology* 158 (2023) 108837. <https://doi.org/10.1016/j.optlastec.2022.108837>.
- [24] Y. Liang, Z.Y. Liao, L.L. Zhang, M.W. Cai, X.S. Wei, J. Shen, A review on coatings deposited by extreme high-speed laser cladding: processes, materials, and properties, *Optics & Laser Technology* 164 (2023) 109472. <https://doi.org/10.1016/j.optlastec.2023.109472>.
- [25] M.-N. Bold, N. Schmitt, J.H. Schleifenbaum, Application of the 3D-EHLA process for agile alloy development, (2022).